Challenges in Manufacturing and Identification of Rare Earth Free Synchronous Machines

Stephan Goehner*, Julius Kesten*, Simon Frank*, Martin Doppelbauer*, Marc Hiller*, Andreas Liske*
*Institute of Electrical Engineering (ETI), Karlsruhe Institute of Technology, Karlsruhe, Germany
Email: stephan.goehner@kit.edu

***Abstract*—This work compares a synchronous reluctance machine (SynRM) to a permanent magnet assisted SynRM (PMaSynRM) with identical rotor geometry and additional AlNiCo magnets. Thus, no rare earth elements are required for both machines. Design validation requires the manufacturing of these machines and identification of their characteristics. However, commissioning and identification present additional challenges. The SynRM's rotor position sensor cannot be aligned using the induced voltage method because there is no induced voltage when idling due to the lack of rotor excitation. Considering the PMaSynRM, the demagnetization issues of AlNiCo magnets during manufacturing of electric machines are discussed, and a magnetizing approach for a fully assembled electrical machine is presented. The proposed solutions are applied to machine prototypes to compare the characteristics with and without magnets considering flux linkages and torque.**

I. Introduction

Electric drive systems continue to gain importance and market shares in vehicle propulsion. However, these systems typically rely on rare earth enabled permanent magnet synchronous machines (PMSM) for torque generation. These materials pose both economical and environmental risks, since they are expensive, supplied only by few countries and only a small percentage of them is being recycled [1].

To mitigate these risks, alternate machine topologies are investigated. This work focuses on the SynRM and PMaSynRM. In SynRMs, torque generation relies solely on the difference in magnetic conductivity between the rotor's d- and q-axis. The PMaSynRM employs so-called semi hard magnets, such as AlNiCo or ferrite alloys. Both magnet types do not rely on rare earth materials. AlNiCo magnets typically present with higher remanence B_{rem} than ferrite alloys, but have smaller coercivity H_{c}. A comparison between an AlNiCo and a ferrite magnet's behavior is presented in Fig. 1. In the figure, the difference in B_{rem} and H_{c} is visible. While the remanence of the AlNiCo magnet lies beyond $1\,\mathrm{T}$, the ferrite is only at $0.4\,\mathrm{T}$. However, the ferrite has a linear behavior throughout the entirety of the second quadrant of the BH plane. The critical field strength of the AlNiCo magnet H_{crit} is displayed as a dashed line in the figure. It denotes the minimal magnetic field strength threshold at which permanent demagnetization of the magnet occurs. Thus, H_{crit} is an important quantity to consider in both the design stage and during operation of the machine [2], [3].

This work was in part financed through the Ministry of Science, Research, and Arts of the Federal State of Baden-Württemberg, Germany, in the framework of "Innovationscampus Mobilität der Zukunft"

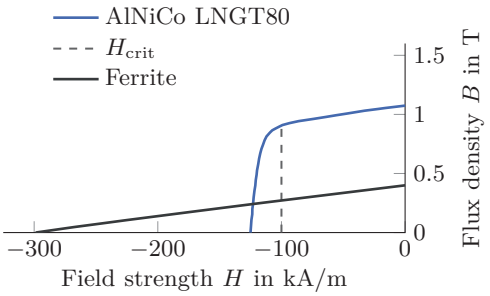


Fig. 1. BH curves of the AlNiCo LNGT80 used in this work and a high-performance ferrite.

While SynRMs suffer from poor power factor and therefore require oversized inverters, PMaSynRMs mitigate this problem partially, improving the power factor compared to SynRM. Therefore, adding rare earth free magnets to a SynRM rotor design allows an improvement in power density of the drive system. The scope of this work is to directly compare a PMaSynRM and SynRM employing a high reluctance torque rotor design based on the authors' previous work [4], [5]. The focus lies on the achievable output torque and the behavior of the current dependent flux linkages Ψ_{d} and Ψ_{q} rather than the machines' efficiency maps. The specific rotor design allows the direct comparison of the machine's performance with and without magnets.

Owing to the small coercivity of the AlNiCo LNGT80 magnets used in the PMaSynRM, its rotor is partly demagnetized prior to assembly. This poses a challenge in design and manufacturing of rare earth free PMaSynRMs, since the magnets' operating points in the assembled state differ from the load acting on the magnets in the rotor in the unassembled state. Due to this, the rotor cannot be magnetized with a separate magnetizing fixture, making the investigation of alternative magnetization setups necessary. This work proposes to magnetize the rotor "in situ", i.e. while it is mounted in the stator.

The paper is structured as follows: Sec. II presents the mathematical machine model used and the key data of the investigated machine designs. Sec. III discusses the challenges faced during testing and presents the authors' solutions to deal with them. The magnetizing approach for the PMaSynRM is presented and the SynRM specific considerations in machine testing are discussed. In Sec. IV the measurement results are

Authorized licensed use limited to: KIT Library. Downloaded on October 28,2026 at 08:40:52 UTC from IEEE Xplore. Restrictions apply.

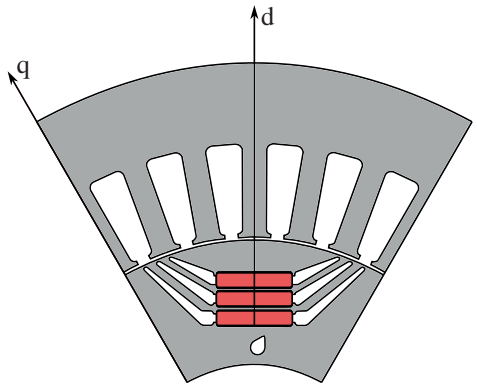


Fig. 2. Cross-section of the investigated machine: the red area marks the possible mounting position for permanent magnets

presented and discussed. The conclusions of this work are given in Sec. V.

II. Fundamentals

The electrical behavior of the three-phase star-connected SynRM and PMaSynRM is described using the voltage equations in the rotor-oriented reference frame:

$$\begin{aligned} v_\mathrm{d} &= R_\mathrm{s} \cdot i_\mathrm{d} + \frac{\mathrm{d}\Psi_\mathrm{d}(i_\mathrm{d}, i_\mathrm{q})}{\mathrm{d}t} - \omega \cdot \Psi_\mathrm{q}(i_\mathrm{d}, i_\mathrm{q}) \\ v_\mathrm{q} &= R_\mathrm{s} \cdot i_\mathrm{q} + \frac{\mathrm{d}\Psi_\mathrm{q}(i_\mathrm{d}, i_\mathrm{q})}{\mathrm{d}t} + \omega \cdot \Psi_\mathrm{d}(i_\mathrm{d}, i_\mathrm{q}) \end{aligned} \tag{1}$$

Here, v are the voltages and i the currents of the respective axis. R_s denotes the ohmic resistance of the stator winding and ω is the rotor's electrical speed. The flux linkages Ψ_d and Ψ_q define the machine's magnetic properties. The inner torque T_i of the machine is given by:

$$T_\mathrm{i} = \frac{3}{2} \cdot p \cdot (\Psi_\mathrm{d} \cdot i_\mathrm{q} - \Psi_\mathrm{q} \cdot i_\mathrm{d}), \tag{2}$$

where p denotes the number of pole pairs.

Fig. 2 shows the investigated machines' cross-section. The triangular hole in the rotor towards the shaft is required to assemble the rotor's segments with the correct skewing angle. For the PMaSynRM, AlNiCo magnets are added in the red area of the flux barriers while they remain empty in the SynRM. Table I shows the design parameters of the machines.

III. Challenges in Machine Commissioning and Identification

Since the design enables operation either as SynRM or PMaSynRM, rotors with and without permanent magnets were manufactured – enabling a comparison of the performance. For the comparison, the machine characteristics are evaluated using the constant speed method (CSM) with a conventional back-to-back test bench setup that will be discussed in Sec. IV. However, the manufacturing and commissioning process have several additional challenges compared to conventional PMSMs that will be addressed in this section.

TABLE I
Parameters of the Investigated Machines

Parameter	Value
Active length	70 mm
Bore Diameter	90 mm
Air Gap Length	0.5 mm
Number of Pole Pairs	3
Number of Slots	36
Rotor Segments	5
Skew Angle	10°
Magnets (only PMaSynRM)	AlNiCo LNGT80
Maximum Speed	5000 min^{-1}
Rated Current	70 A (RMS)
Rated DC-Link Voltage	48 V

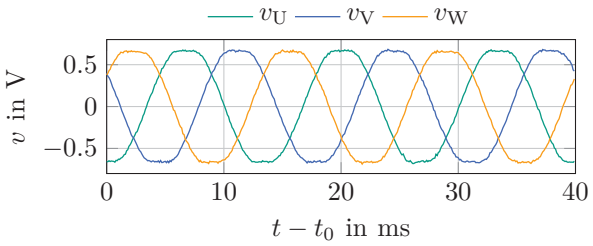


Fig. 3. Induced voltage of the demagnetized PMaSynRM at 1500 min^{-1}

A. De- and Remagnetization of the PMaSynRM

The comparable low coercivity of AlNiCo LNGT80 leads to demagnetization of the PMaSynRM's rotor when it is not fitted to the stator, due to the large load imposed on the magnets through the magnetic resistance of the surrounding air. To demonstrate this, the machine's induced voltage at no load was measured directly after gluing the magnets to rotor and placing it in the stator of the machine. Fig. 3 shows the measured voltage at a speed of 1500 min^{-1}. The amplitude of the induced voltage and consequently the permanent magnet flux linkage Ψ_PM are less than 10 % of the finite element analysis (FEA) result of a fully magnetized rotor.

The rotor has to be magnetized while assembled in the stator because demagnetization is expected as soon as it is removed from it. FEA analysis shows that to apply the magnetizing field of the used AlNiCo LNGT80 of $H_\mathrm{mag} \approx 480\,\mathrm{kA/m}$ to all the magnets in the rotor, a positive d-current pulse $i_\mathrm{d,mag} \approx 4\,\mathrm{kA}$ is required in the stator. To achieve currents in this range, the institute's double pulse test bench [6] is used with *FZ3600R17HP4* IGBT modules from *Infineon* and an extended DC link capacitance. The module is rated for a repetitive surge current of 7.2 kA with a pulse duration of 1 ms [7]. Fig. 4 shows the electrical setup used to create a current pulse in the α-axis: Terminal V and W of the machine are shorted. Assuming a symmetrical machine, the current of phase U splits symmetrical at the star-point and results in the desired current space vector. This series-parallel connection of the machine phases replaces the load inductance of the double pulse test bench.

The rotor's d-axis is aligned with the α-axis of the stator and mechanically locked during the magnetization as shown

ISBN: 978-3-8007-6612-3

@ VDE VERLAG GMBH · Berlin · Offenbach
Authorized licensed use limited to: KIT Library. Downloaded on October 28,2026 at 08:40:52 UTC from IEEE Xplore. Restrictions apply.

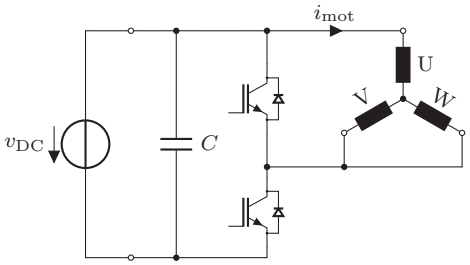


Fig. 4. Modified double pulse setup to magnetize the machine

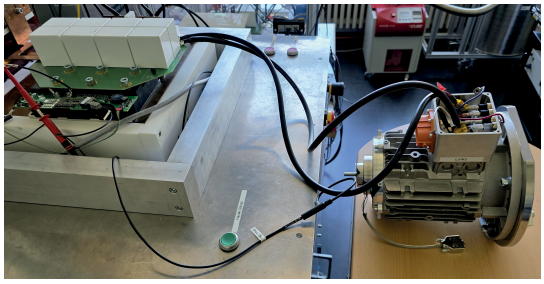


Fig. 5. PMaSynRM connected to the double pulse test bench

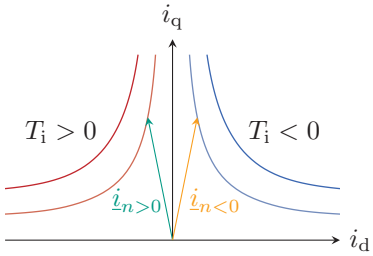


Fig. 8. Constant torque contour lines in the dq-current space for a SynRM

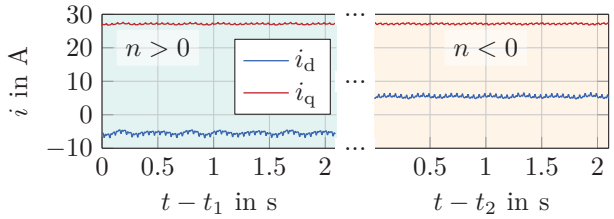


Fig. 9. dq-currents during the proposed alignment procedure for positive and negative speed after offset calibration

in Fig. 5. Fig. 6 shows the current pulse applied to the machine measured with a *CWT Mini HF30B* Rogowski coil from *PEM*. It rises in approximately 1 ms to 4.25 kA. The rotor magnetization is then evaluated using the induced voltage presented in Fig. 7. The voltage amplitude increases by a factor of 7.5 compared to the voltage before magnetization shown in Fig. 3 yielding $\Psi_{\mathrm{PM}} = 10.5\,\mathrm{mVs}$. This corresponds to approximately 67 % of the FEA result for a fully magnetized rotor.

B. Alignment of the Rotor Position Sensor of the SynRM

Current control in the rotor-oriented reference frame, that is used for the CSM measurements, requires information about the absolute position of the rotor relative to the stator. The machine prototypes feature rotor position sensors that are mounted in an arbitrary position relative to the rotor's d-axis and thus need to be aligned. The state-of-the-art method from the PMSM [8] cannot be used for the SynRM because it does not show an induced voltage when idling. Alternatively, a current in the α-axis of the machine can be applied to the unloaded machine. It is assumed that the rotor aligns with the axis of lowest reluctance. However, friction and position dependent torque ripple lead to a deviation from an exact alignment.

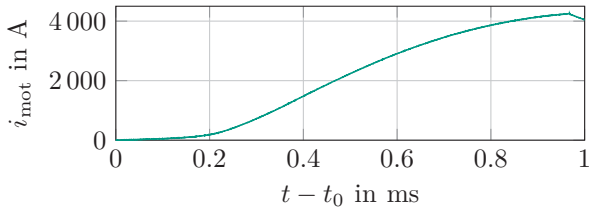


Fig. 6. Current pulse measured during magnetization of the motor with the double pulse test bench

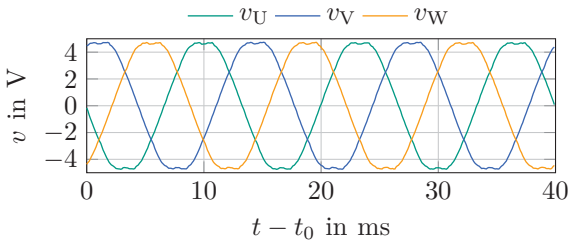


Fig. 7. Induced voltage of the magnetized PMaSynRM at $1500\,\mathrm{min}^{-1}$

To avoid such a deviation, this work proposes a different method that is based on the SynRM's torque symmetry for positive and negative d-currents:

$$T_{\mathrm{i}}(i_{\mathrm{d}}, i_{\mathrm{q}}) = -T_{\mathrm{i}}(-i_{\mathrm{d}}, i_{\mathrm{q}}) \tag{3}$$

The proposed method applies a voltage space vector to the stator winding of the unloaded machine starting with zero speed. Similar to the method of a constant current in the α-axis, the rotor is expected to align its q-axis close to the current space vector after an initial transient. Next, the rotor is accelerated to a constant speed n using a rotating voltage space vector determined with V/f-control, and the currents are recorded. Then, the speed is reversed, and the currents recorded again. Assuming the load torque is symmetrical for positive and negative speeds, according to (3) the q-current should be identical while the d-current changes its sign as illustrated in Fig. 8. This is achieved by modifying the offset angle of the rotor position sensor accordingly. Fig. 9 shows the measured dq-currents after applying the proposed calibration of the offset for positive and negative speed.

ISBN: 978-3-8007-6612-3

@ VDE VERLAG GMBH · Berlin · Offenbach
Authorized licensed use limited to: KIT Library. Downloaded on October 28,2026 at 08:40:52 UTC from IEEE Xplore. Restrictions apply.

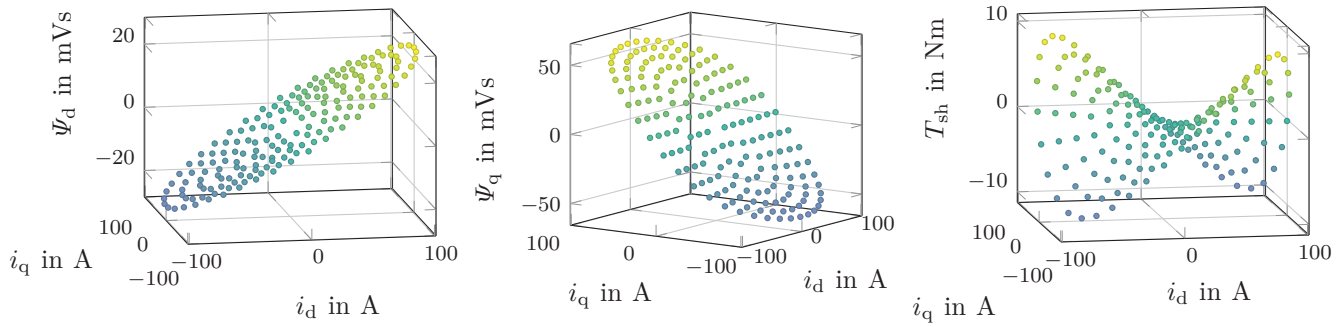


Fig. 10. Result of the design characterization for the SynRM at $900\,\mathrm{min}^{-1}$

C. Alignment of the Rotor Position Sensor of the Demagnetized PMaSynRM

As described in Sec. III-A, the rotor's d-axis needs to be aligned with the stator's α-axis for the magnetization process. Due to the low magnetization, the position sensor alignment using the induced voltage [8] does not yield reliable results.

However, the alignment does not need to be very precise because AlNiCo LNGT80 as part of the AlNiCo9 class is an anisotropic material that has only little remanence when magnetized in the non-preferred direction [9]. After magnetization, the conventional induced voltage approach can be used for precise alignment of the rotor position sensor.

IV. Results

The machines are evaluated using the test bench platform proposed in [10]. A *Dewetron DEWE3-PA8-RM* power analyzer is used to record all quantities. The electrical measurements use a *TRION3-1810M-PA* module with *Signaltec CT 100* current transducers. Torque and rotor position are measured with a *Kistler 4503B* shaft torque sensor rated for $50\,\mathrm{Nm}$. For the measurements, both designs are operated with a DC link voltage of $60\,\mathrm{V}$. The design comparison includes besides the flux linkage and torque evaluation also the analysis of the demagnetization of the PMaSynRM in the rated current range.

A. Synchronous Reluctance Machine

After manufacturing, the SynRM is mounted to the test bench and its rotor position sensor aligned as proposed in Sec. III-B. Fig. 10 shows the flux linkages Ψ_d, Ψ_q and the shaft torque T_sh of the SynRM identified at $900\,\mathrm{min}^{-1}$ using the CSM. Saturation is visible for Ψ_q for higher currents and Ψ_d shows some cross saturation.

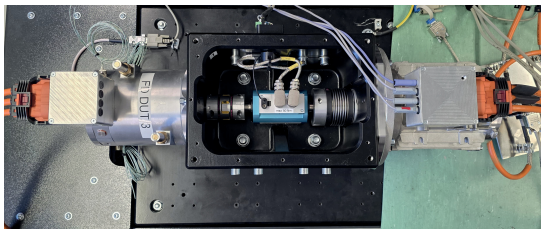


Fig. 11. PMaSynRM mounted to the test bench

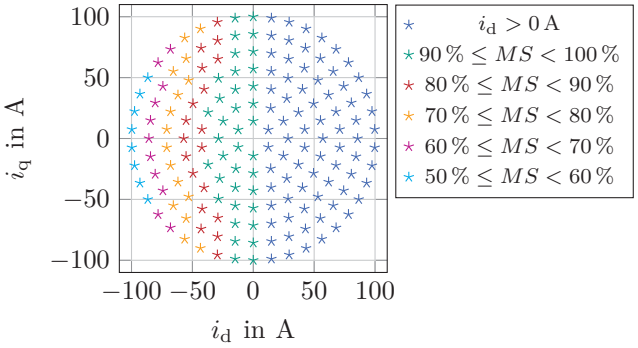


Fig. 12. Current targets used for machine characterization: the color highlights the expected magnetization state after applying the current to a fully magnetized the machine

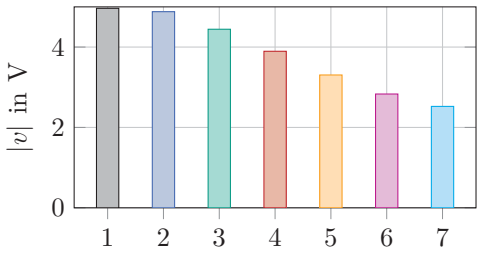


Fig. 13. Induced voltage after measuring different current targets: 1 denotes the initial induced voltage. The further color coding corresponds to Fig. 12.

The measured torque is near $0\,\mathrm{Nm}$ for pure d- or q-current as expected, and the flux linkages show the expected reflection symmetries. This indicates, the proposed position sensor alignment is able to align the rotor position sensor precisely.

B. PMaSynRM

Fig.11 shows the magnetized PMaSynRM mounted to the test bench. Its position sensor is aligned using the induced voltage method [8]. Compared to the SynRM, the temporal order in which the current targets are measured needs to be considered due to expected demagnetization during operation with negative d-currents. Fig. 12 shows the current targets used to characterize the PMaSynRM. The color indicates

ISBN: 978-3-8007-6612-3

@ VDE VERLAG GMBH · Berlin · Offenbach
Authorized licensed use limited to: KIT Library. Downloaded on October 28,2026 at 08:40:52 UTC from IEEE Xplore. Restrictions apply.

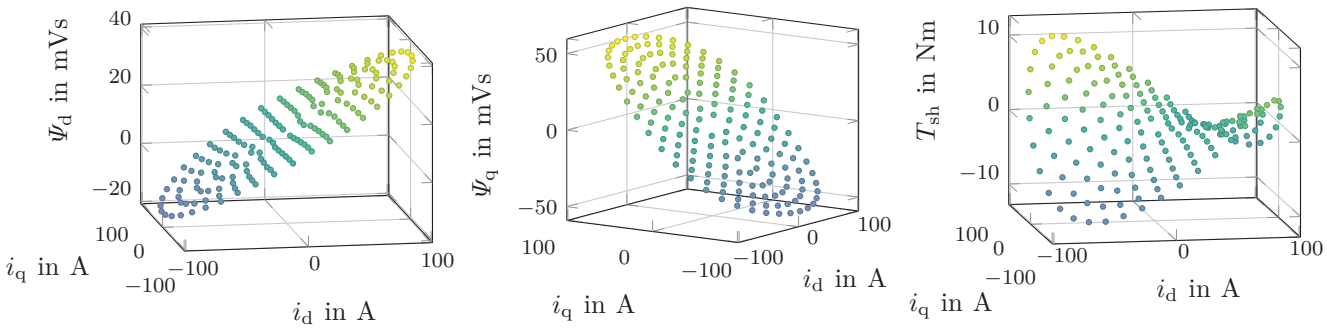


Fig. 14. Result of the design characterization for the PMaSynRM at $900\,\mathrm{min}^{-1}$

the expected rotor magnetization state (MS) based on FEA simulations after a given operating point is applied.

To achieve the maximum machine performance, the characterization starts with only positive d-currents and then continues with the current targets in the order of their expected MS. Fig. 13 shows the induced voltage measured for no load at $1500\,\mathrm{min}^{-1}$ after each MS interval was measured. The decreased voltage clearly indicates demagnetization after applying negative d-currents.

The result of the design characterization is presented in Fig. 14, which results when the current targets are measured in the previously described order. The motoring peak torque current target was measured again after completing all presented current targets to highlight the influence of the order of measurement. The measured torque is reduced by $3.4\,\%$ from $10.5\,\mathrm{Nm}$ to $10.1\,\mathrm{Nm}$ at the lower MS. The identified Ψ_d also reduces by $1.9\,\mathrm{mVs}$ while Ψ_q remains unchanged.

C. Comparison of the Designs

While the flux linkage in the q-axis is similar for both machines, the d-axis clearly shows the influence of the magnetization that causes a positive offset for Ψ_d of the PMaSynRM. For high negative i_d the demagnetization of the PMaSynRM is visible in the steeper descend of Ψ_d. Magnetization of the rotor bridges in the SynRM causes a high slope of Ψ_d for small i_d, that is not visible for the PMaSynRM because the magnet's leakage flux already saturates the bridges.

Because the SynRM has no magnets, there is just reluctance torque present, that does not change when the current vector is rotated by $180°$. In the PMaSynRM, synchronous and reluctance torque are present. They partly cancel out for $i_\mathrm{d} > 0\,\mathrm{A}$ and reinforce for $i_\mathrm{d} < 0\,\mathrm{A}$. Considering the maximum possible torque, the magnetized PMaSynRM prototype reaches a $13\,\%$ higher torque of $10.6\,\mathrm{Nm}$ in generating mode compared to the pure SynRM due to the additional synchronous torque. When motoring, the torque increases by $16\,\%$ over the SynRM.

Even when the lowest magnetization state is considered that has to be expected in the rated current range, the PMaSynRM achieves $12\,\%$ higher peak torque than the SynRM in motoring mode. Also, the power factor increases for this point. At the evaluated speed of $900\,\mathrm{min}^{-1}$ it changes from 0.59 (SynRM) to 0.68 (PMaSynRM).

V. Conclusion

This work presents challenges faced when building rare earth element free synchronous machine prototypes. The evaluated machine design can be build as SynRM or PMaSynRM when magnets are added to the rotor. For operation as SynRM, a new position sensor alignment procedure is proposed that considers harmonics in the flux linkages and enables a precise alignment.

The SynRM has a lower torque density and worse power factor compared to the design with magnets. The PMaSynRM remains rare earth element free by using semi hard magnetic AlNiCo LNGT80 for the rotor magnets. These show a significantly lower coercivity compared to rare earth magnets, that results in demagnetization during manufacturing when the magnets face the high magnetic resistance of air. Measurements of the induced voltage demonstrate that the initially demagnetized rotor can be significantly magnetized with the same stator that is used for operation. The required current pulse is generated with a double pulse test bench that is typically used for semiconductor characterization.

Future work includes the development of an operating strategy considering the demagnetization of the PMaSynRM and efficiency comparison with the SynRM over the torque-speed-range. The PMaSynRM characterization results can be used as feedback for the machine design process to further improve the magnetization and demagnetization behavior during operation.

References

[1] European Commission. Directorate General for Internal Market, Industry, Entrepreneurship and SMEs., *Study on the critical raw materials for the EU 2023: final report*. eng. LU: Publications Office, 2023.

[2] T. A. Huynh, M.-F. Hsieh, K.-J. Shih, and H.-F. Kuo, "An Investigation Into the Effect of PM Arrangements on PMaSynRM Performance," *IEEE Transactions on Industry Applications*, vol. 54, no. 6, pp. 5856–5868, Jan. 2018, ISSN: 0093-9994. DOI: 10.1109/TIA.2018.2853042.

[3] S. S. Maroufian and P. Pillay, "PM Assisted Synchronous Reluctance Machine Design Using AlNiCo Magnets," in *2017 IEEE International Electric Machines and Drives Conference (IEMDC)*, IEEE, May 2017, pp. 1–6, ISBN: 978-1-5090-4281-4. DOI: 10.1109/IEMDC.2017.8002163.

Authorized licensed use limited to: KIT Library. Downloaded on October 28,2026 at 08:40:52 UTC from IEEE Xplore. Restrictions apply.

[4] J. Kesten, F. Frölich, F. Wittemann, *et al.*, "Design Approach for a Novel Multi Material Variable Flux Synchronous Reluctance Machine without Rare Earth Magnets," in *2022 International Conference on Electrical Machines (ICEM)*, IEEE, 2022, pp. 2304–2310, ISBN: 978-1-6654-1432-6. DOI: 10.1109/ICEM51905.2022.9910780.

[5] J. Freyer, J. Kesten, and T. Ketelhut, "Design and Development of a Modular Motor-Gearbox-Unit for an Electric Light Vehicle," en, in *Proceedings of the FISITA - Technology and Mobility Conference Europe 2023*, Barcelona, Spain: FISITA, 2023. DOI: 10.46720/fwc2023-lvp-017.

[6] F. Stamer, R. Schwendemann, and M. Hiller, "A multi-dimensional full automatic power semiconductor test bench for accurate semiconductor loss calculation," in *PCIM Europe 2019; International Exhibition and Conference for Power Electronics, Intelligent Motion, Renewable Energy and Energy Management*, May 2019, pp. 1–8.

[7] Infineon Technologies AG. "FZ3600R17HP4 — 1700 V, 3600 A single switch IGBT module - Infineon Technologies." (), [Online]. Available: https://www.infineon.com/cms/en/product/power/igbt/igbt-modules/fz3600r17hp4/ (visited on 06/02/2025).

[8] J. Richter, A. Dollinger, and M. Doppelbauer, "Iron loss and parameter measurement of permanent magnet synchronous machines," in *2014 International Conference on Electrical Machines (ICEM)*, Sep. 2014, pp. 1635–1641. DOI: 10.1109/ICELMACH.2014.6960401.

[9] G. Gallicchio, M. D. Nardo, M. Palmieri, and F. Cupertino, "Analysis, design and optimization of hysteresis clutches," *IEEE Open Journal of Industry Applications*, vol. 1, pp. 258–269, 2020, ISSN: 2644-1241. DOI: 10.1109/OJIA.2020.3042884.

[10] S. Goehner, A. Oerder, T. Zeller, *et al.*, "A modular rapid prototyping test bench platform for accelerated electric drive research," in *PCIM Conference 2025*, in press, Nuremberg: VDE Verlag GmbH, May 6, 2025, pp. 971–980, ISBN: 978-3-8007-6541-6. DOI: 10.30420/566541123.

Authorized licensed use limited to: KIT Library. Downloaded on October 28,2026 at 08:40:52 UTC from IEEE Xplore. Restrictions apply.

BIOGRAPHIES

Stephan Goehner studied electrical engineering and information technology at Karlsruhe Institute of Technology (KIT), Karlsruhe, Germany, where he received his B.Sc. (2020) and M.Sc. (2022). Since 2023 he is research assistant in the research group for control of power electronics systems at Institute of Electrical Engineering (ETI) at KIT. His main research topics are modeling, parameter identification and control of electric drives with focus on synchronous machines. In his recent work, he examined flux linkage identification of permanent magnet and electrically excited synchronous machines using steady state and locked rotor tests.

Julius Kesten received his M.Sc in Mechatronics and Information Technology 2020 from the Karlsruhe Institute of Technology (KIT), Germany. Since 2020 he works at the Institute of Electrical Engineering at the KIT. His research interests include the design of synchronous reluctance and variable flux machines and the numerical optimization of electric machines.

Simon Frank received his M.Sc. from KIT in 2020 and is currently research associate at KIT ETI. His recent research focuses on power electronics at cryogenic temperatures.

Martin Doppelbauer was born in Altenhundem, Germany. He received the Dipl.-Ing. and Dr.-Ing. degrees in electrical engineering from the University of Dortmund, Germany in 1990 and 1995, respectively. He was with the companies Danfoss Bauer in Esslingen and SEW Eurodrive in Bruchsal, Germany, as Senior Manager for electric motor development. Since 2011 he is full professor at the Institute of Electrical Engineering (ETI) at the KIT. He holds a chair for Hybrid Electric Vehicles. Martin Doppelbauer is also active in national and international standardization and the chairman of IEC Technical Committee 2 Rotating Electrical Machines.

Marc Hiller received the diploma degree from the Technische Universität Darmstadt, Darmstadt, Germany, in 1993, and the Ph.D. degree from the Universität der Bundeswehr München, Neubiberg, Germany, in 2008, both in electrical engineering. Since 2005, he has been with the Drive Technology Division, Sector Industry, Siemens AG, Nuremberg, Germany, where he was the Project Manager in the development of industrial medium-voltage drives. His research interests include modern power-hardware-in-the-loop converters, modeling of electrical drives and grids, and grid connected converter, energy storage integration, and the control of power semiconductors. Dr. Hiller has been the Chair of Power Electronic Systems with the Karlsruhe Institute of Technology, Karlsruhe, Germany, since 2015.

Andreas Liske received the Dipl.-Ing. degree in electrical engineering and communication technology from the Technical University of Karlsruhe and the PhD degree in electrical engineering from the Karlsruhe Institute of technology (KIT) in 2010 and 2020 respectively. Since 2010 he was lecturer and since 2012 senior engineer at the Institute of Electrical Engineering (ETI) at the KIT. In 2020 he became assistant professor and group-leader of the research team “Control and modelling of power electronics systems” at the very same institute. Dr. Liske teaches 4 lectures in power electronics, modeling, and control of electrical machines at KIT.

ISBN: 978-3-8007-6612-3

@ VDE VERLAG GMBH · Berlin · Offenbach
Authorized licensed use limited to: KIT Library. Downloaded on October 28,2026 at 08:40:52 UTC from IEEE Xplore. Restrictions apply.